ELSEVIER

SCIENCE DIRECT

Physics Letters B 599 (2004) 148–158

PHYSICS LETTERS B

www.elsevier.com/locate/physletb

Observation of the decays $B^0 \to K^+\pi^-\pi^0$ and $B^0 \to \rho^- K^+$

Belle Collaboration

P. Chang [x], K. Abe [g], K. Abe [am], T. Abe [g], H. Aihara [ao], Y. Asano [as], V. Aulchenko [a], T. Aushev [k], T. Aziz [ak], S. Bahinipati [d], A.M. Bakich [aj], Y. Ban [ad], A. Bay [p], I. Bedny [a], U. Bitenc [l], I. Bizjak [l], A. Bondar [a], A. Bozek [y], M. Bračko [r,l], J. Brodzicka [y], T.E. Browder [f], M.-C. Chang [x], Y. Chao [x], B.G. Cheon [c], R. Chistov [k], S.-K. Choi [e], Y. Choi [ai], S. Cole [aj], M. Danilov [k], M. Dash [at], L.Y. Dong [i], A. Drutskoy [d], S. Eidelman [a], V. Eiges [k], Y. Enari [t], F. Fang [f], S. Fratina [l], N. Gabyshev [a], A. Garmash [ae], T. Gershon [g], G. Gokhroo [ak], B. Golob [q,l], R. Guo [v], N.C. Hastings [g], H. Hayashii [u], M. Hazumi [g], T. Higuchi [ao], L. Hinz [p], T. Hokuue [t], Y. Hoshi [am], W.-S. Hou [x], Y.B. Hsiung [x,1], H.-C. Huang [x], K. Inami [t], A. Ishikawa [g], R. Itoh [g], H. Iwasaki [g], M. Iwasaki [ao], Y. Iwasaki [g], J.H. Kang [au], J.S. Kang [n], S.U. Kataoka [u], N. Katayama [g], H. Kawai [b], T. Kawasaki [aa], H.R. Khan [ap], H. Kichimi [g], H.J. Kim [o], J.H. Kim [ai], S.K. Kim [ah], T.H. Kim [au], P. Koppenburg [g], S. Korpar [r,l], P. Križan [q,l], P. Krokovny [a], A. Kuzmin [a], Y.-J. Kwon [au], S.E. Lee [ah], T. Lesiak [y], J. Li [ag], S.-W. Lin [x], J. MacNaughton [j], G. Majumder [ak], F. Mandl [j], D. Marlow [ae], T. Matsumoto [aq], A. Matyja [y], W. Mitaroff [j], H. Miyake [ac], H. Miyata [aa], R. Mizuk [k], D. Mohapatra [at], T. Mori [ap], T. Nagamine [an], Y. Nagasaka [h], E. Nakano [ab], M. Nakao [g], H. Nakazawa [g], Z. Natkaniec [y], S. Nishida [g], O. Nitoh [ar], S. Ogawa [al], T. Okabe [t], S. Okuno [m], S.L. Olsen [f], W. Ostrowicz [y], H. Ozaki [g], P. Pakhlov [k], H. Park [o], N. Parslow [aj], L.S. Peak [aj], L.E. Piilonen [at], A. Poluektov [a], N. Root [a], M. Rozanska [y], H. Sagawa [g], Y. Sakai [g], O. Schneider [p], J. Schümann [x], S. Semenov [k], K. Senyo [t], M.E. Sevior [s], H. Shibuya [al], V. Sidorov [a], A. Somov [d], R. Stamen [g], S. Stanič [as,2], M. Starič [l], K. Sumisawa [ac], T. Sumiyoshi [aq], S. Suzuki [af], O. Tajima [an], F. Takasaki [g], K. Tamai [g], N. Tamura [aa], M. Tanaka [g], Y. Teramoto [ab], T. Tsukamoto [g], S. Uehara [g], K. Ueno [x], T. Uglov [k], Y. Unno [b], S. Uno [g], G. Varner [f], K.E. Varvell [aj], S. Villa [p], C.C. Wang [x], C.H. Wang [w], M.-Z. Wang [x], M. Watanabe [aa], B.D. Yabsley [at], Y. Yamada [g], A. Yamaguchi [an], Y. Yamashita [z], M. Yamauchi [g], J. Ying [ad], C.C. Zhang [i], J. Zhang [g], Z.P. Zhang [ag], D. Žontar [q,l]

[a] *Budker Institute of Nuclear Physics, Novosibirsk, Russia*

doi:10.1016/j.physletb.2004.07.063

[b] Chiba University, Chiba, Japan
[c] Chonnam National University, Kwangju, South Korea
[d] University of Cincinnati, Cincinnati, OH, USA
[e] Gyeongsang National University, Chinju, South Korea
[f] University of Hawaii, Honolulu, HI, USA
[g] High Energy Accelerator Research Organization (KEK), Tsukuba, Japan
[h] Hiroshima Institute of Technology, Hiroshima, Japan
[i] Institute of High Energy Physics, Chinese Academy of Sciences, Beijing, PR China
[j] Institute of High Energy Physics, Vienna, Austria
[k] Institute for Theoretical and Experimental Physics, Moscow, Russia
[l] J. Stefan Institute, Ljubljana, Slovenia
[m] Kanagawa University, Yokohama, Japan
[n] Korea University, Seoul, South Korea
[o] Kyungpook National University, Taegu, South Korea
[p] Swiss Federal Institute of Technology of Lausanne, EPFL, Lausanne, Switzerland
[q] University of Ljubljana, Ljubljana, Slovenia
[r] University of Maribor, Maribor, Slovenia
[s] University of Melbourne, Victoria, Australia
[t] Nagoya University, Nagoya, Japan
[u] Nara Women's University, Nara, Japan
[v] National Kaohsiung Normal University, Kaohsiung, Taiwan
[w] National United University, Miao Li, Taiwan
[x] Department of Physics, National Taiwan University, Taipei, Taiwan
[y] H. Niewodniczanski Institute of Nuclear Physics, Krakow, Poland
[z] Nihon Dental College, Niigata, Japan
[aa] Niigata University, Niigata, Japan
[ab] Osaka City University, Osaka, Japan
[ac] Osaka University, Osaka, Japan
[ad] Peking University, Beijing, PR China
[ae] Princeton University, Princeton, NJ, USA
[af] Saga University, Saga, Japan
[ag] University of Science and Technology of China, Hefei, PR China
[ah] Seoul National University, Seoul, South Korea
[ai] Sungkyunkwan University, Suwon, South Korea
[aj] University of Sydney, Sydney, NSW, Australia
[ak] Tata Institute of Fundamental Research, Bombay, India
[al] Toho University, Funabashi, Japan
[am] Tohoku Gakuin University, Tagajo, Japan
[an] Tohoku University, Sendai, Japan
[ao] Department of Physics, University of Tokyo, Tokyo, Japan
[ap] Tokyo Institute of Technology, Tokyo, Japan
[aq] Tokyo Metropolitan University, Tokyo, Japan
[ar] Tokyo University of Agriculture and Technology, Tokyo, Japan
[as] University of Tsukuba, Tsukuba, Japan
[at] Virginia Polytechnic Institute and State University, Blacksburg, VA, USA
[au] Yonsei University, Seoul, South Korea

Received 28 June 2004; accepted 23 July 2004

Available online 7 September 2004

Editor: M. Doser

E-mail address: pchang@phys.ntu.edu.tw (P. Chang).

[1] On leave from Fermi National Accelerator Laboratory, Batavia, IL, USA.

[2] On leave from Nova Gorica Polytechnic, Nova Gorica, Slovenia.

Abstract

We report the observation of B^0 decays to the $K^+\pi^-\pi^0$ final state using a data sample of 78 fb^{-1} collected by the Belle detector at the KEKB e^+e^- collider. With no assumptions about intermediate states in the decay, the branching fraction is measured to be $(36.6^{+4.2}_{-4.3} \pm 3.0) \times 10^{-6}$. We also search for B decays to intermediate two-body states with the same $K^+\pi^-\pi^0$ final state. Significant B signals are observed in the $\rho(770)^- K^+$ and $K^*(892)^+\pi^-$ channels, with branching fractions of $(15.1^{+3.4+1.4+2.0}_{-3.3-1.5-2.1}) \times 10^{-6}$ and $(14.8^{+4.6+1.5+2.4}_{-4.4-1.0-0.9}) \times 10^{-6}$, respectively. The first error is statistical, the second is systematic and the third is due to the largest possible interference. Contributions from other possible two-body states will be discussed. No CP asymmetry is found in the inclusive $K^+\pi^-\pi^0$ or $\rho^- K^+$ modes, and we set 90% confidence level bounds on the asymmetry of $-0.12 < A_{CP} < 0.26$ and $-0.18 < A_{CP} < 0.64$, respectively.

PACS: 13.25.Hw; 14.40.Nd

1. Introduction

Recently, observations of large branching fractions for three-body charmless hadronic decays of B mesons have been reported by the B factory experiments [1–6]. In the mesonic decays $B \to K\pi^+\pi^-$ and $B \to KK^+K^-$, a large fraction of the decays proceed through intermediate two-body decay processes, such as $B^+ \to K^*(892)^0\pi^+$, $K^*(892)^0 \to K^+\pi^-$ and $B^+ \to \phi K^+, \phi \to K^+K^-$. However, higher mass $K^+\pi^-$, $\pi^+\pi^-$ and K^+K^- states may contribute but are not clearly identified due to limited statistics. Moreover, the broad K^+K^- mass spectrum above 1.5 GeV/c^2 in $B^+ \to K^+K^+K^-$ suggests a large non-resonant $B^+ \to K^+K^+K^-$ contribution. In the baryonic decay $B^+ \to p\bar{p}K^+$, a simple phase-space model fails to describe the $p\bar{p}$ mass spectrum, which may be explained by a baryonic form factor model [7] or by an additional, unknown resonance around 2 GeV/c^2. These studies of three-body decays have provided new information on the mechanism of B meson decay, and provide opportunities to search for unknown B meson decays and to understand the interference between them. In this Letter we report on a study of B meson decays to $K^+\pi^-\pi^0$, independently of possible intermediate states. In addition, we also present results of a search for quasi-two-body intermediate states. Inclusion of charge conjugate modes is always implied in this Letter unless otherwise specified. The results are obtained from data collected by the Belle detector [8] at the KEKB asymmetric e^+e^- storage ring [9]. The data sample corresponds to an integrated luminosity of 78 fb^{-1} and contains 85.0 million $B\bar{B}$ pairs at the $\Upsilon(4S)$ resonance.

2. Apparatus and event selection

The Belle detector is a large-solid-angle general purpose spectrometer based on a 1.5 T superconducting solenoidal magnet. Charged tracks are reconstructed with a three layer double-sided silicon vertex detector (SVD) and a central drift chamber (CDC) that consists of 50 layers segmented into 6 axial and 5 stereo superlayers. The CDC covers the polar angle range between 17° and 150° in the laboratory frame and, together with the SVD, gives a transverse momentum resolution of $(\sigma_{p_t}/p_t)^2 = (0.0019 p_t)^2 + (0.0030)^2$, where p_t and σ_{p_t} are in GeV/c. Charged hadron identification is performed using a combination of three devices: an array of 1188 aerogel Čerenkov counters (ACC) covering the momentum range 1–4 GeV/c, a time-of-flight scintillation counter system (TOF) for track momenta below 1.5 GeV/c, and dE/dx information from the CDC for particles with low or high momenta. Situated between these devices and the solenoid coil is an electromagnetic calorimeter (ECL) consisting of 8736 CsI(Tℓ) crystals with a typical front-surface cross section of 5.5×5.5 cm^2 and a depth of $16.2X_0$. The ECL provides a photon energy resolution of $(\sigma_E/E)^2 = 0.013^2 + (0.0007/E)^2 + (0.008/E^{1/4})^2$, where E and σ_E are in GeV. An instrumented iron flux return outside the solenoid coil is used for muon and K_L detection. A de-

tailed description of the Belle detector can be found in Ref. [8].

Charged tracks are required to come from the collision point and have transverse momenta, p_t, above 100 MeV/c. The accepted tracks are then refitted with their vertex position constrained to the run-averaged profile of B meson decay vertices in the transverse plane. Charged K and π mesons are identified by combining information from the CDC (dE/dx), the TOF and the ACC to form a $K(\pi)$ likelihood $L_K(L_\pi)$. Discrimination between kaons and pions is achieved through the likelihood ratio $L_K/(L_\pi + L_K)$. The performance of the charged hadron identification is studied using a kinematically selected high momentum D^{*+} data sample, where $D^{*+} \to D^0\pi^+$, $D^0 \to K^-\pi^+$. We measure the pion and kaon identification efficiencies and their fake rates as functions of track momentum. The typical kaon and pion identification efficiencies for 1 GeV/c tracks are $(87.9 \pm 0.6)\%$ and $(89.4 \pm 0.6)\%$, respectively. The rate for true pions to be misidentified as kaons is $(9.0 \pm 0.5)\%$, while the rate for true kaons to be misidentified as pions is $(10.0 \pm 0.6)\%$. Charged tracks which are positively identified as electrons and muons are rejected. Candidate neutral pions are selected by requiring the two-photon invariant mass to be in the mass window $0.118\ \text{GeV}/c^2 < M(\gamma\gamma) < 0.150\ \text{GeV}/c^2$, corresponding to $\pm 2.5\sigma$ mass resolution with momentum above 2 GeV/c. The momentum of each photon is then readjusted, constraining the mass of the photon pair to be the nominal π^0 mass. To reduce the background from soft photons, each photon is required to have energy above 50 MeV and the minimum π^0 momentum is 200 MeV/c.

Candidate B mesons are identified using the beam constrained mass,

$$M_{\text{bc}} = \sqrt{E_{\text{beam}}^2 - P_B^2},$$

and the energy difference, $\Delta E = E_B - E_{\text{beam}}$, where E_{beam} is run-dependent and determined from $B \to D^{(*)}\pi$ events, and P_B and E_B are the momentum and energy of the B candidate in the $\Upsilon(4S)$ rest frame. The parameterizations of the signal in M_{bc} and ΔE are determined by a GEANT-based Monte Carlo (MC) [10] simulation of non-resonant $B^0 \to K^+\pi^-\pi^0$ decays, and various quasi-two-body decays to the $K^+\pi^-\pi^0$ final state. The signal parameterization is verified using the data and MC samples of $B^+ \to \bar{D}^0\pi^+$, $\bar{D}^0 \to K^+\pi^-\pi^0$ candidates. Our MC overestimates the M_{bc} resolution by 8% but underestimates the ΔE resolution by 9% to 15%, depending on the kinematics of the $K^+\pi^-\pi^0$ events. The MC based signal probability density functions (PDF) are readjusted accordingly.

The Gaussian width of the signal in M_{bc} is about 3.0 MeV/c^2, which is primarily due to the beam energy spread. The ΔE distribution is found to be asymmetric, with a tail on the lower side due to γ interactions with material in front of the calorimeter, and shower leakage out of the back side of the crystals. As a result, the ΔE resolution and the tail distribution strongly depend on the π^0 energy; the ΔE width ranges from 20 to 33 MeV. In the inclusive $K^+\pi^-\pi^0$ study, since the π^0 energy distribution for the signal is not known a priori, the data is divided into three samples: $P(\pi^0) < 0.5$ GeV/c, $0.5\ \text{GeV}/c < P(\pi^0) < 1.5\ \text{GeV}/c$ and $P(\pi^0) > 1.5$ GeV/c. The ΔE distribution in each sample is modeled with a Crystal Ball lineshape [11] with parameters determined from MC. Events with $M_{\text{bc}} > 5.2\ \text{GeV}/c^2$ and $|\Delta E| < 0.3$ GeV are selected for the final analysis. The signal region is defined as $M_{\text{bc}} > 5.27\ \text{GeV}/c^2$ and $-0.10\ \text{GeV} < \Delta E < 0.08$ GeV. Events located in the region $M_{\text{bc}} < 5.265\ \text{GeV}/c^2$ are defined as sideband events and are used for background studies. When more than one B^0 candidate is found in an event, the candidate having the smallest sum of the χ^2 from the vertex fit and π^0 mass constrained fit is selected.

The dominant background for three-body B decay events comes from the $e^+e^- \to q\bar{q}$ continuum, where $q = u, d, s$ or c. In order to reduce this background, several shape variables are chosen to distinguish spherical $B\bar{B}$ events from jet-like continuum events. Five modified Fox–Wolfram moments [12] and a measure of the momentum transverse to the event thrust axis ($S_\perp$) [13] are combined into a Fisher discriminant. The PDFs for this discriminant and $\cos\theta_B$, where θ_B is the angle between the B flight direction and the beam direction in the $\Upsilon(4S)$ rest frame, are obtained using events in the signal and sideband regions from MC simulations for signal and $q\bar{q}$ background. These two variables are then combined to form a likelihood ratio $\mathcal{R} = \mathcal{L}_s/(\mathcal{L}_s + \mathcal{L}_{q\bar{q}})$, where $\mathcal{L}_{s(q\bar{q})}$ is the product of signal ($q\bar{q}$) probability densities. Continuum background is suppressed by requiring $\mathcal{R} > 0.9$, based on a study of the signal signif-

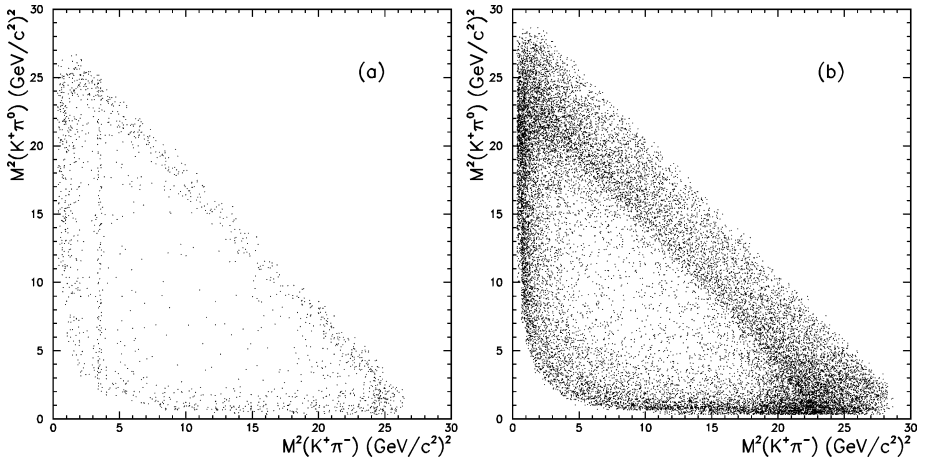

Fig. 1. Dalitz plot of $B^0 \to K^+\pi^-\pi^0$ candidates from (a) the B signal region and (b) the $M_{\rm bc}$ sideband region. The enhancement around $M^2(K^+\pi^-) = 3.5\ (\mathrm{GeV}/c^2)^2$ is from $B^0 \to \bar{D}^0\pi^0$ events.

icance ($N_S/\sqrt{N_S+N_B}$) using a MC sample, where N_S and N_B are signal and background yields, respectively. This $\mathcal{R}$ requirement retains 45% of the signal and removes 97% of the continuum events. The effect of the $\mathcal{R}$ cut is studied by comparing $B^+ \to \bar{D}^0\pi^+$ in data and MC, for different values of $\mathcal{R}$. A systematic error of 3% is obtained for the $\mathcal{R}$ cut.

Fig. 1 shows the Dalitz plot distribution of $K^+\pi^-\pi^0$ candidates in the ΔE–$M_{\rm bc}$ signal region and $M_{\rm bc}$ sideband region. $K^+\pi^-\pi^0$ candidates populate the three edges of the Dalitz plot, indicating the existence of quasi-two-body intermediate states. Moreover, there is an enhancement near $M^2(K^+\pi^-) = 3.5\ (\mathrm{GeV}/c^2)^2$ in Fig. 1(a), which is due to the decay $B^0 \to \bar{D}^0\pi^0$, $\bar{D}^0 \to K^+\pi^-$. To restrict the study to charmless B decays, events with a $K^+\pi^-$ mass within $50\ \mathrm{MeV}/c^2$ of the nominal $\bar{D}^0$ mass are rejected.

3. Inclusive $K^+\pi^-\pi^0$ yield

The final signal yields are obtained from fits to the ΔE and $M_{\rm bc}$ distributions. In addition to continuum background, the final sample contains background from $\Upsilon(4S) \to B\bar{B}$ events. The ΔE and $M_{\rm bc}$ shapes of this $B\bar{B}$ background are modeled with smooth histograms, generated from a large GEANT based $B\bar{B}$ MC sample, which includes $b \to c$ transitions and charmless B decays. Backgrounds from $b \to c$ transitions populate in the low ΔE region while backgrounds from $B \to K\pi$ and $B \to \rho\pi$ contribute in the regions $\Delta E > 0.2\,\mathrm{GeV}$ and $\Delta E \sim 0.05\,\mathrm{GeV}$, respectively. Small contributions from other charmless B decays are also included to model the $B\bar{B}$ background shape. The continuum ΔE background shape is modeled by either a first or second order polynomial, determined from the $M_{\rm bc}$ sideband data. The continuum $M_{\rm bc}$ background shape is modeled with an ARGUS function [14] with parameters determined from events outside the ΔE signal region. One-dimensional binned likelihood fits to ΔE and $M_{\rm bc}$ are performed using signal, continuum background and $B\bar{B}$ background PDFs for events in the $M_{\rm bc}$ and ΔE signal region, respectively. Since the $M_{\rm bc}$ shapes from $B\bar{B}$ background are difficult to distinguish from signal shapes, the signal yields are estimated using the ΔE

Table 1
Fit results for inclusive $K^+\pi^-\pi^0$ events. Columns 3 and 4 list the signal yield and the statistical significance. The $B\bar{B}$ fraction is fixed to the MC expectation in the $M_{\rm bc}$ fit, while it is allowed to float in the ΔE fit. The last row shows the sum of the three ΔE fits

	π^0 momentum (GeV/c)	Signal yield	Significance
$M_{\rm bc}$ fit	No requirement	369 ± 35	11.4
ΔE fit	$p < 0.5$	$31^{+13}_{-12} \pm 4$	2.6
	$0.5 < p < 1.5$	$93 \pm 22^{+6}_{-7}$	4.6
	$p > 1.5$	$262 \pm 36 \pm 13$	7.8
	Sum	$386 \pm 44^{+14}_{-15}$	9.4

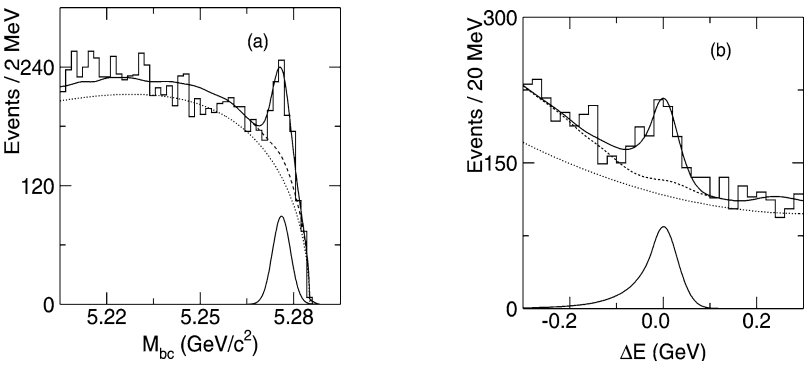

Fig. 2. (a) $M_{\rm bc}$ and (b) ΔE distributions for inclusive $K^+\pi^-\pi^0$ events. Solid lines in the figures represent the result of the fit and the signal contribution. Dashed lines show the total background contribution, while dotted lines indicate the continuum contribution. The ΔE lines in (b) show the sum of the fit results to the three subsamples. A sizeable $B^0 \to K^+\pi^-$ and $B^+ \to K^+\pi^0$ feed-down at $\Delta E > 0.2$ GeV is found in the MC. This contribution is included in the fit.

fit and cross checked by the $M_{\rm bc}$ fit, where the $B\bar{B}$ background fraction is fixed to the MC expectation.

Table 1 summarizes the fit result of the inclusive $K^+\pi^-\pi^0$ sample with the statistical significance (Σ) defined as $\sqrt{-2\ln(\mathcal{L}_0/\mathcal{L}_{\rm max})}$, where $\mathcal{L}_0$ and $\mathcal{L}_{\rm max}$ denote the likelihood values at zero yield and the best fit numbers, respectively. The sum of the signal yield from the ΔE fits to the three subsamples, 386 ± 44, is consistent with the yield from the $M_{\rm bc}$ fit, 369 ± 35, which has a smaller signal efficiency than the ΔE fit due to the tighter ΔE requirement. The corresponding projections of the fits are shown in Fig. 2. Furthermore, a consistent result is obtained when the $B\bar{B}$ fraction is fixed according to the MC expectation.

4. Two-body intermediate states

We perform a search for quasi-two-body decays in the $K^+\pi^-\pi^0$ final state, including B decays to a pseudoscalar (K or π) and a vector meson ($\rho(770)$ or $K^*(892)$) and other possible intermediate states with higher mass resonances. Three pseudoscalar-vector (PV) modes are considered: $K^*(892)^0\pi^0$, $K^*(892)^+\pi^-$, and $\rho(770)^-K^+$. Fig. 3 shows the B signal yields from the ΔE fit as functions of $K^+\pi^-$, $K^+\pi^0$ and $\pi^-\pi^0$ masses. To eliminate cross-talk between decay modes, each two-body mass is examined after requiring the other two-body masses to be large (> 1.6 GeV/c^2 for $K\pi$ and > 1.1 GeV/c^2 for $\pi^-\pi^0$). The ΔE signal PDFs are obtained from MC simulations of $B^0 \to K_0^*(1430)^0\pi^0$, $B^0 \to K_0^*(1430)^+\pi^-$ and $B^0 \to \rho(770)^-K^+$ for the $K^+\pi^-$, $K^+\pi^0$ and $\pi^-\pi^0$ cases, respectively.

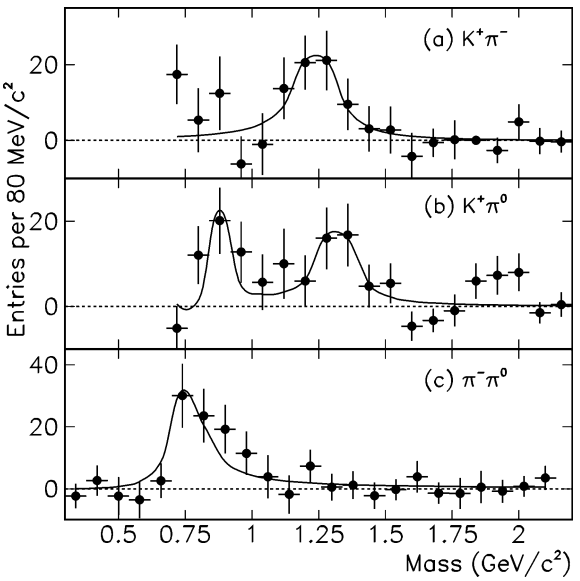

Fig. 3. B yields from ΔE fits as a function of (a) $K^+\pi^-$, (b) $K^+\pi^0$ and (c) $\pi^-\pi^0$. Each two-body mass is examined after requiring the other two-body masses to be large (> 1.6 GeV/c^2 for $K\pi$ and > 1.1 GeV/c^2 for $\pi^-\pi^0$). Dotted points are data; the superimposed curves in (b) and (c) are the projection curves based on $K^*(892)^+$ and $\rho(770)^-$. The enhancements between 1.1 to 1.5 GeV/c^2 in (a) and (b) are modeled with Breit–Wigner functions.

In the $K^+\pi^-$ sample, a large enhancement is observed between 1.0 and 1.6 GeV/c^2, peaking around 1.2 to 1.4 GeV/c^2. More structure is observed in the $K^+\pi^0$ spectrum. An enhancement is seen in the

$K^*(892)^+$ mass region, in the region from 1.2 to 1.4 GeV/c^2 and possibly between 1.8 and 2.1 GeV/c^2. In the $\pi^-\pi^0$ sample, a clear excess is seen in the $\rho(770)^-$ signal region. Although the enhancement between 1.1 and 1.6 GeV/c^2 is observed in both $K^+\pi^-$ and $K^+\pi^0$ spectra, these higher mass $K\pi$ states cannot be identified without performing an angular analysis that requires much more data. Possible candidates are $K^*(1410)$, $K_0^*(1430)$ and $K_2^*(1430)$. Earlier studies of $B^+ \to K^+\pi^+\pi^-$ [1] and $B^0 \to K^0\pi^+\pi^-$ [5] decays also observed large quasi-two-body B decays with $K_x^*(K\pi)$ mesons in the final state. If the enhancements observed in the $K^+\pi^0$ mass spectrum are due to such K_x^* mesons, one would expect the same resonances to appear in the $K^0\pi^+$ mode. The first two enhancements seen in the $K^+\pi^0$ mode (Fig. 3(b)) are indeed observed in the $B^0 \to K^0\pi^+\pi^-$ analysis [2]. However, the third enhancement, between 1.8 and 2.1 GeV/c^2, does not appear in the $K^0\pi^+\pi^-$ mode. This enhancement, which has a signal yield of 22^{+9}_{-8} events and a significance of 3σ, may be either a statistical fluctuation, or originate from $K_2(1820)$, $K_4^*(2045)$ or from a doubly Cabibbo suppressed D^+ decay. More data are needed to clarify the current situation.

To further understand the possible resonances, we study the distributions of $\cos\theta_H$, where the helicity angle θ_H is defined as the angle between the direction of the candidate B meson and the K^+ (π^0) direction in the $K^*(\rho)$ rest frame. Fig. 4 shows the B yields as a function of $\cos\theta_H$ for events in the $K^*(892)^+, \rho(770)^-, K_x^*(K\pi)$ signal region. The $\cos\theta_H$ distributions for the first two modes are consistent with those of $B^0 \to$ pseudoscalar vector (PV) decays, as expected for $B^0 \to K^*(892)^+\pi^-$ and $B^0 \to \rho(770)^-K^+$. Note that the asymmetry in the $\cos\theta_H$ distributions is due to the inefficiency of low momentum π^0 reconstruction. Since π^0s from $B^0 \to \rho^-K^+$ decays are more energetic than those from $B^0 \to K^*(892)^+\pi^-$, the asymmetric effect is less pronounced. The $\cos\theta_H$ distributions for the K_x^{*0} and K_x^{*+} modes favor a scalar behavior.

5. Yield for various states

We measure $B^0 \to K^+\pi^-\pi^0$ decay rates for the three PV modes, events in the two $K_x^*\pi$ regions,

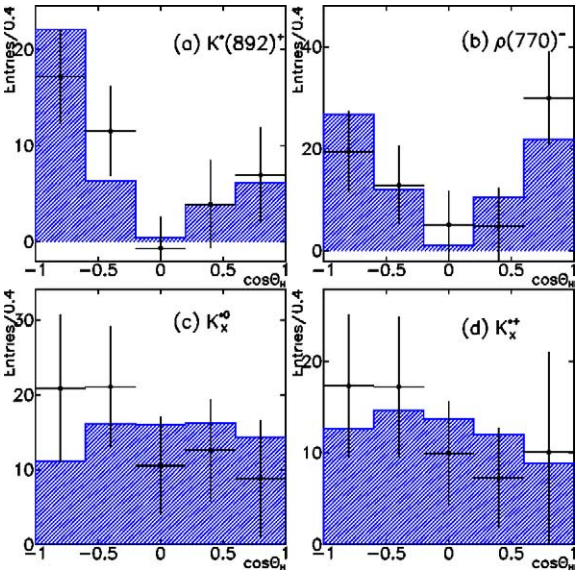

Fig. 4. B signal yields as a function of $\cos\theta_H$ for events in (a) $K^*(892)^+$, (b) $\rho(770)^-$, (c) K_x^{*0} and (d) K_x^{*+} regions. Points are data and histograms are the expectations from (a) $B^0 \to K^*(892)^+\pi^-$, (b) $B^0 \to \rho(770)^-K^+$ and (c), (d) B decays to a scalar and a pseudoscalar meson.

and the central region of the Dalitz plot with two-body masses above 2.0 GeV/c^2. Candidate $K^*(892)$ and $\rho(770)^-$ mesons are identified by requiring the $K^+\pi^{-(0)}$ and $\pi^-\pi^0$ masses to be in the range 820–980 MeV/c^2 and 570–970 MeV/c^2, respectively. To further reduce background, a selection of $|\cos\theta_H| > 0.3$ is applied to the vector meson candidates. In the two $K_x^{*0(+)}\pi$ regions, we require 1.1 GeV/c^2 < $M(K^+\pi^{-(0)}) < 1.6$ GeV/c^2. B meson candidates are then selected from the inclusive $K^+\pi^-\pi^0$ events after applying all analysis cuts, including the appropriate two-body mass vetos to avoid cross talk. The signal PDFs are obtained from MC simulations for all six channels, where a scalar hypothesis is used to model $K_x^*\pi$.

Fig. 5 shows the $M_{\rm bc}$ and ΔE distributions, and their corresponding fit curves, for the three PV modes. No signal yield is seen in the $K^{*0}\pi^0$ channel but significant signals are observed for the $K^{*+}\pi^-$ and ρ^-K^+ modes; the yields measured from the ΔE fits are 38 ± 11 and 77^{+18}_{-17} events, with statistical significances of 3.8σ and 4.9σ, respectively. As for events in the central region of the Dalitz plot and the two K_x^* regions, Fig. 6 shows their $M_{\rm bc}$ and ΔE dis-

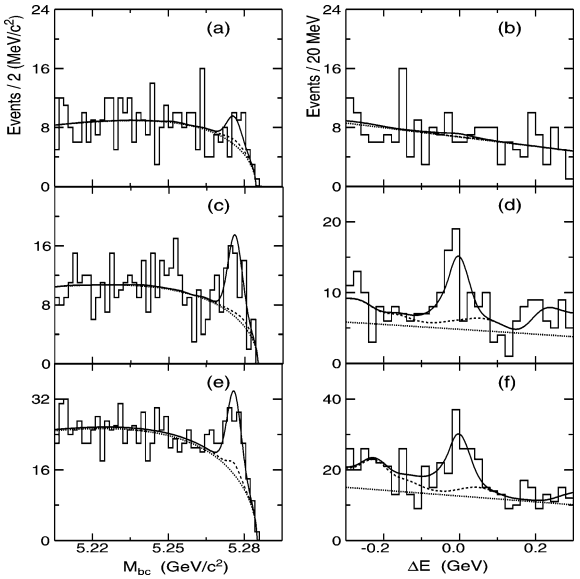

Fig. 5. $M_{\rm bc}$ and ΔE distributions for (a), (b) $K^{*0}\pi^0$, (c), (d) $K^{*+}\pi^-$ and (e), (f) ρ^+K^- events. The superimposed solid curves represent the corresponding fits. Dashed lines are the background projections and the dotted lines show the continuum $q\bar{q}$ contribution. Enhancements in the projection curves at $\Delta E > 0.2$ GeV and $\Delta E \sim 0.05$ GeV in (d) and (f) are due to $B \to K\pi$ and $B \to \rho\pi$ decays, respectively.

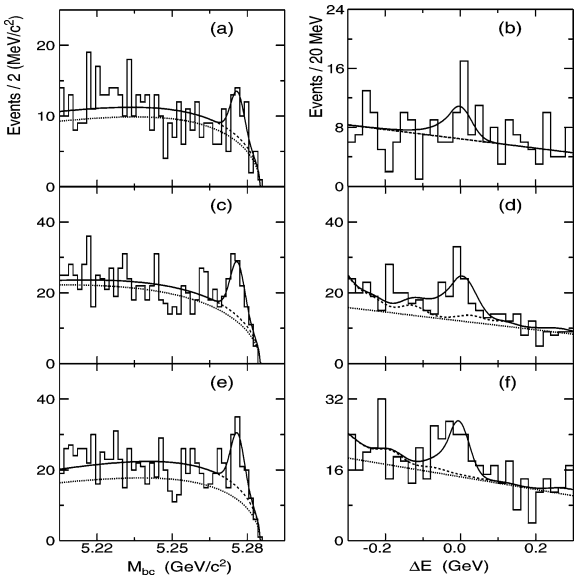

Fig. 6. $M_{\rm bc}$ and ΔE distributions for events in different regions of the Dalitz plots: (a), (b) the central region, (c), (d) $K_x^{*0}\pi^0$ region and (e), (f) $K_x^{*+}\pi^-$ region. The superimposed solid curves represent the corresponding fits. Dashed lines are the background projections and the dotted lines show the continuum $q\bar{q}$ contribution. Enhancements in the projection curves at $\Delta E > 0.2$ GeV in (d) and (f) are due to $B \to K\pi$ decays.

tributions with the fit curves superimposed. Based on the ΔE fit, there are 67 ± 17 and 52 ± 15 signal events in $K_x^{*0}\pi^0$ and $K_x^{*+}\pi^-$, respectively. Since events in these $K_x^*\pi$ regions cannot be positively identified, their reconstruction efficiencies are determined without assumptions about the intermediate two-body states. Although a yield of around 20 events is obtained from both the ΔE and $M_{\rm bc}$ fits for the central region of the Dalitz plot, the statistical significance is below 3σ and, hence, an upper limit is reported. The reconstruction efficiency is obtained from a phase-space decay model.

The number of feed-across events from high mass K_x^* to the $K^*(892)$ region is estimated from the B yields in the $1.1\ \text{GeV}/c^2 < M(K^+\pi^0) < 1.6\ \text{GeV}/c^2$ region, and the Breit–Wigner distribution, modeled with a mass of $1.326\ \text{GeV}/c^2$ and a mean of $252\ \text{MeV}/c^2$. We find a contribution of 1 event. Assuming no interference, the $K^*(892)^+\pi^-$ yield is estimated to be 37 ± 11. The possible effect of interference is studied using a Monte Carlo simulation that assumes the three PV decays and two $K_x^*\pi$ states. We compare the yields with and without interference. After varying the relative phase of each channel, and taking into account the non-uniform reconstruction efficiency over the Dalitz plot, the largest deviation is $^{+16\%}_{-6\%}$ for $K^*(892)^+\pi^-$ and $^{+13\%}_{-14\%}$ for ρ^-K^+. These two numbers are used to estimate the systematic error arising from interference.

6. Systematic uncertainties

The systematic error for each signal yield is estimated by varying each parameter of the fit functions by $\pm 1\sigma$ from the measured values. The shifts in signal yield are then added in quadrature. The typical fit systematic error for the inclusive decay is around 4%. Signal efficiencies are first obtained from MC simulations, and then corrected by comparing data and MC predictions for other processes. The efficiency for the inclusive $K^+\pi^-\pi^0$ signal is estimated from the weighted sum of the efficiencies for the possible two-body intermediate states shown in Fig. 3, where the

sub-decay branching fraction for each two-body state is not included. The uncertainty on this inclusive efficiency is 5%, determined by comparing the reconstruction efficiencies on various two-body modes. The π^0 reconstruction efficiency is verified by comparing the π^0 decay angular distribution with the MC prediction, and by measuring the ratio of the branching fractions of two η decay channels: $\eta \to \gamma\gamma$ and $\eta \to \pi^0\pi^0\pi^0$. The typical systematic error for π^0 detection is 3%. The systematic errors on the charged track reconstruction are estimated to be $\sim 2\%$ using partially reconstructed D^* events, and verified by comparing the ratio of $\eta \to \pi^+\pi^-\pi^0$ to $\eta \to \gamma\gamma$ in data with MC expectations. The final systematic errors on the reconstruction efficiencies, including charged particle and π^0 detection, particle identification and the $\mathcal{R}$ cut, range from 7 to 14% for the quasi-two-body decays and is 8.2% for the inclusive $K^+\pi^-\pi^0$ channel.

7. Branching fractions

Table 2 summarizes the fit results for each reconstructed decay channel. The branching fractions and upper limits are calculated assuming that B^+B^- and $B^0\bar{B}^0$ are produced with equal probability. The systematic errors on the branching fractions combine the systematic errors for the reconstruction efficiencies and the ΔE fit with the uncertainty from the number of $B\bar{B}$ events. Since no signal is seen in the $K^{*0}\pi^0$ mode, and the signal yield in the central region of the Dalitz plot is not significant, upper limits are computed at the 90% confidence level (C.L.) based on the observed number of events in the signal region, and the background level found by the fit; both the statistical and systematic errors are taken into account [15]. With 85.0 million $B\bar{B}$ events, we measure the branching fraction to be $(36.6^{+4.2}_{-4.1}(\text{stat.}) \pm 3.0(\text{syst.})) \times 10^{-6}$ for the inclusive $B^0 \to K^+\pi^-\pi^0$ decay, without assumptions about intermediate two-body states. The branching fractions of $B^0 \to K^*(892)^+\pi^-$ and $B^0 \to \rho^- K^+$ decay are measured to be $(14.8^{+4.6+1.5+2.4}_{-4.4-1.0-0.9}) \times 10^{-6}$ and $(15.1^{+3.4+1.4+2.0}_{-3.3-1.5-2.1}) \times 10^{-6}$, where the first error is statistical, the second is systematic and the third corresponds to the largest uncertainty from the interference between different states. Finally, the $B^0 \to K^+\pi^-\pi^0$ decay branching fractions in the $K^{*0}_x\pi^0$ and $K^{*+}_x\pi^-$ regions are measured to be $(6.1^{+1.6+0.5}_{-1.5-0.6}) \times 10^{-6}$ and $(5.1 \pm 1.5^{+0.6}_{-0.7}) \times 10^{-6}$, respectively.

8. Search for CP violation

Using the large signals observed in the inclusive $B^0 \to K^+\pi^-\pi^0$ and $B^0 \to \rho^- K^+$ modes, we search for direct CP violation by dividing the data into two subsets, according to the charge of the kaon. The asymmetry, defined as $A_{CP} = \frac{N_{\bar{B}} - N_B}{N_{\bar{B}} + N_B}$, is then computed using the B signal yields obtained from ΔE fits. Following the same fitting procedure, we observe 179^{+31}_{-30} $K^+\pi^-\pi^0$ events and 207^{+32}_{-31} $K^-\pi^+\pi^0$

Table 2
Summary of the $B^0 \to K^+\pi^-\pi^0$ search. We present signal yields, efficiencies, and their statistical significances for the inclusive mode, the three intermediate channels of $B \to$ PV decays and the other three regions of the Dalitz plot. The sub-decay branching fractions of the three PV modes are included in the efficiencies for the three $B \to$ PV modes. Branching fractions and/or upper limits are shown in the last two columns. In the branching fractions, the first error is statistical and the second systematic. The third error for $K^*(892)^+\pi^-$ and $\rho^- K^+$ corresponds to the largest uncertainty from the interference between different states. The last channel, $K^+\pi^-\pi^0_{NR}$, indicates the non-resonant $B^0 \to K^+\pi^-\pi^0$ decay

Channel	Yield	Eff. (%)	Sig.	BF (10^{-6})	UL (10^{-6})
$K^+\pi^-\pi^0$	386 ± 44	12.4	9.4	$36.6^{+4.2}_{-4.1} \pm 3.0$	–
$K^*(892)^0\pi^0$	2^{+11}_{-10}	6.7	0.3	$0.4^{+1.9}_{-1.7} \pm 0.1$	3.5
$K^*(892)^+\pi^-$	37 ± 11	2.9	3.8	$14.8^{+4.6+1.5+2.4}_{-4.4-1.0-0.9}$	–
$\rho^- K^+$	77^{+18}_{-17}	6.0	4.9	$15.1^{+3.4+1.4+2.0}_{-3.3-1.5-2.1}$	–
$K^{*0}_x\pi^0$	67 ± 17	12.9	4.2	$6.1^{+1.6+0.5}_{-1.5-0.6}$	–
$K^{*+}_x\pi^-$	52 ± 15	11.9	3.7	$5.1 \pm 1.5^{+0.6}_{-0.7}$	–
$K^+\pi^-\pi^0_{NR}$	22^{+10}_{-9}	4.1	2.5	$5.7^{+2.7+0.5}_{-2.5-0.4}$	9.4

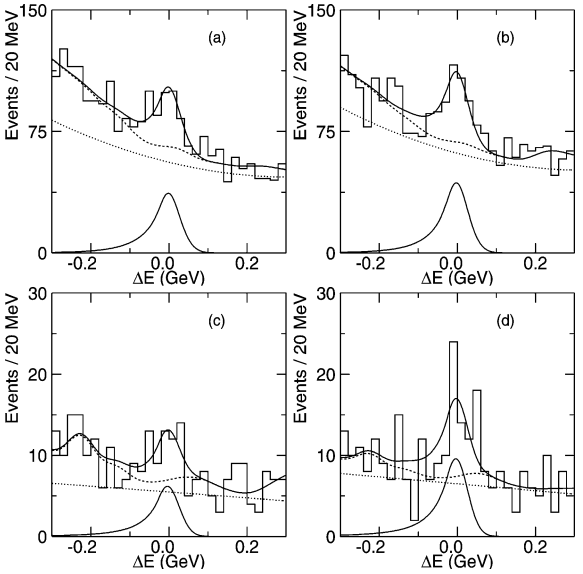

Fig. 7. ΔE distributions for the (a) $K^+\pi^-\pi^0$, (b) $K^-\pi^+\pi^0$, (c) ρ^-K^+ and (d) ρ^+K^- samples. The superimposed solid curves represent the corresponding fits and signal projections. Dashed lines are the background projections and dotted lines show the continuum $q\bar{q}$ contribution. Enhancements in the projection curves at $\Delta E > 0.2$ GeV are due to $B \to K\pi$ decays.

events, while the ΔE fit yields 30^{+12}_{-11} ρ^-K^+ events and 47^{+13}_{-12} ρ^+K^- events (see Fig. 7). The possible reconstruction bias in A_{CP} is studied by checking the inclusive $\bar{D}^0 \to K^+\pi^-$ and $D^0 \to K^-\pi^+$ yields in data. The obtained systematic error is 0.5%. Adding this 0.5% error in quadrature with the fitting systematic error, obtained by varying each parameter in the PDFs by 1σ, gives the total systematic error. Finally, the CP asymmetry is calculated to be $A_{CP} = 0.07 \pm 0.11 \pm 0.01$ for the inclusive mode, and $A_{CP} = 0.22^{+0.22+0.06}_{-0.23-0.02}$ for $B^0(\bar{B}^0) \to \rho^\mp K^\pm$. We also set 90% confidence intervals on the asymmetry of $-0.12 < A_{CP} < 0.26$ for the inclusive mode, and $-0.18 < A_{CP} < 0.64$ for $B^0 \to \rho^\mp K^\pm$.

9. Conclusions

In summary, we have studied the charmless hadronic decays, $B^0 \to K^+\pi^-\pi^0$, which is observed for the first time. Our results show that the branching fraction of $B^0 \to K^+\pi^-\pi^0$ is $(64 \pm 10)\%$ and $(78 \pm 15)\%$ of that of $B^+ \to K^+\pi^-\pi^+$ [2,4] and $B^0 \to K^0\pi^-\pi^+$ [2,5], respectively. The $K^+\pi^-\pi^0$ signal candidates populate the edge of the Dalitz plot, indicating the existence of quasi-two-body states. For the $K^+\pi^-\pi^0$ final state, we have observed signals in the $K^{*+}\pi^-$ and ρ^-K^+ samples but no significant $K^{*0}\pi^0$ signal is seen. The ρ^-K^+ branching fraction is close to the $K^{*+}\pi^-$ branching fraction, where our measurement is consistent with the earlier CLEO result [5]. However, our ρ^-K^+ result is twice that of BaBar's measurement [6]. We also report the B decay rates in other regions of the Dalitz plot without assumptions about the presence of two-body intermediate states. In the future, significantly more data will be collected at Belle, which will enable us to perform a full Dalitz analysis, allowing us to identify other quasi-two-body states and extract their relative phases. Finally, we performed a search for direct CP violation in the inclusive and $B^0 \to \rho^-K^+$ channels. No evidence of CP violating asymmetry is seen and 90% C.L. limits on A_{CP} are set.

Acknowledgements

We wish to thank the KEKB accelerator group for the excellent operation of the KEKB accelerator. We acknowledge support from the Ministry of Education, Culture, Sports, Science, and Technology of Japan and the Japan Society for the Promotion of Science; the Australian Research Council and the Australian Department of Education, Science and Training; the National Science Foundation of China under contract No. 10175071; the Department of Science and Technology of India; the BK21 program of the Ministry of Education of Korea and the CHEP SRC program of the Korea Science and Engineering Foundation; the Polish State Committee for Scientific Research under contract No. 2P03B 01324; the Ministry of Science and Technology of the Russian Federation; the Ministry of Education, Science and Sport of the Republic of Slovenia; the National Science Council and the Ministry of Education of Taiwan; and the US Department of Energy.

References

[1] A. Garmash, et al., Belle Collaboration, Phys. Rev. D 65 (2002) 092005.

[2] A. Garmash, et al., Belle Collaboration, Phys. Rev. D 69 (2004) 012001.
[3] M. Wang, et al., Belle Collaboration, Phys. Rev. Lett. 92 (2004) 131801.
[4] B. Aubert, et al., BaBar Collaboration, Phys. Rev. Lett. 91 (2003) 051801.
[5] E. Eckhart, et al., CLEO Collaboration, Phys. Rev. Lett. 89 (2002) 251801.
[6] B. Aubert, et al., BaBar Collaboration, Phys. Rev. Lett. 91 (2003) 201802.
[7] C.-K. Chua, W.-S. Hou, S.-Y. Tsai, Phys. Rev. D 65 (2002) 034003;
H.-Y. Cheng, K.-C. Yang, Phys. Rev. D 66 (2002) 014020.
[8] A. Abashian, et al., Belle Collaboration, Nucl. Instrum. Methods A 479 (2002) 117.
[9] S. Kurokawa, E. Kikutani, Nucl. Instrum. Methods A 499 (2003) 1, and other papers included in this volume.
[10] R. Brun, et al., GEANT 3.21, CERN Report No. DD/EE/84-1, 1987.
[11] J.E. Gaiser, et al., Crystal Ball Collaboration, Phys. Rev. D 34 (1986) 711.
[12] The Fox–Wolfram moments were introduced in: G. Fox, S. Wolfram, Phys. Rev. Lett. 41 (1978) 1581;
The modified Fox–Wolfram moments were described in: K. Abe, et al., Phys. Lett. B 511 (2001) 151.
[13] R. Ammar, et al., CLEO Collaboration, Phys. Rev. Lett. 71 (1993) 674.
[14] H. Albrecht, et al., ARGUS Collaboration, Phys. Lett. B 241 (1990) 278.
[15] For the $K^*(892)^0\pi^0$ limit we follow the approach of: G.J. Feldman, R.D. Cousins, Phys. Rev. D 57 (1998) 3873;
Using the implementation of: J. Conrad, et al., Phys. Rev. D 67 (2003) 012002, to include the systematic errors. For the $K^+\pi^-\pi^0_{NR}$ mode this method returns a two-sided interval $[2.0, 9.4] \times 10^{-6}$. Because the significance is less than three, we discard the lower edge of this interval and (conservatively) quote an upper limit of 9.4×10^{-6}.